Soft Matter

Accepted Manuscript

ROYAL SOCIETY OF CHEMISTRY

www.rsc.org/softmatter

ARTICLE TYPE www. rsc.org/xxxxxx | XXXXXXXX

Orientational order of one-patch colloidal particles in two dimensions†

Yasutaka Iwashita,*[a] and Yasuyuki Kimura[a]

Received Xth XXXXXXXXXX 20XX, Accepted Xth XXXXXXXXX 20XX
First published on the web Xth XXXXXXXXXX 200X
DOI: 10.1039/b000000x

We studied the orientational order of one-patch colloidal particles (Janus particles) in a close-packed monolayer. In an experiment on hemispherically patched particles, we realized a highly ordered zigzag stripe pattern by inducing directional growth of the pattern via a phase transition of the solvent. Upon spontaneous ordering by strengthening the inter-patch attraction, however, the particles are trapped in a poorly ordered zigzag pattern, illustrating the importance of controlling kinetics to attain a highly ordered state. The patch-size dependence of an equilibrium orientational order is experimentally observed under moderate inter-patch attraction. We also calculated the equilibrium order against the patch size and attraction in a Monte Carlo simulation. In the simulation, the rather discrete transition between a zigzag stripe, tiling of triangular trimers and tiling of dimers under strong attraction becomes continuous with weakening attraction. The experimental result not only coincides with the simulation qualitatively but also suggests that a particular cluster is selectively formed by nonuniform inter-patch attraction in the experiment. The effect of patch–substrate attraction and commonalities of the order with liquid crystals are also discussed.

1 Introduction

To produce new functional materials, the synthesis of anisotropic colloidal particles with well-defined shapes and interactions has been developed recently.[1,2] Sticky patches can be formed on the surface of a particle by chemically modifying particular regions of the surface.[3,4] Such patchy particles have directional interactions, and thus show unique self-assembly compared with isotropic particles in the form of clusters such as Bernal spirals and micelles,[5–8] crystals such as kagome and diamond,[9–14] and reversible gels and empty liquids.[15,16] The diversity and novelty of the self-assembled structure have attracted the attention of researchers in terms of not only application[15,17] but also the clarification of collective behaviors of natural anisotropic colloids with a patchy character such as proteins.[18–20]

Even for spherical one-patch particles, recent theoretical works have revealed rich crystalline phases with orientational order in two dimensions[14] and three dimensions.[12,21] In the case of a two-dimensional hexagonal monolayer,[14] for example, the ground states are determined by the number of possible attractive bonds per patch, resulting in tiling of dimers for one bond/patch ($\theta_{ap} \leq 30^\circ$), tiling of triangular trimers for two bonds/patch ($30^\circ < \theta_{ap} \leq 60^\circ$) and a zigzag stripe pattern for three bonds/patch ($60^\circ < \theta_{ap} \leq 90^\circ$), where θ_{ap} is the half opening angle of a patch (see Fig. 1 (a)). With decreasing bond energy, the boundaries separating the states shift to larger θ_{ap} and finally a plastic crystal state appears.

Experimental study of such order or crystal often encounters several difficulties. Monodisperse particles with well-defined patches and appropriate inter-patch attraction are required, and it has been theoretically shown that patchy particles are easily trapped in a metastable state upon self-assembly.[7,22,23]

In this article, we experimentally realize various orientational orders of one-patch colloidal particles in a close-packed hexagonal monolayer, and reveal the ordering mechanism by comparing the results of the experiment with those of our numerical simulation. In the experiment, we adopt two different kinetic processes of ordering: (i) spontaneous ordering by tuning the inter-patch attraction via solvent criticality[8] and (ii) induced ordering using phase transition of the solvent and surface activity of the particles (cf. ref.[24]). This experiment exemplifies the significant role of ordering kinetics in realizing a highly ordered pattern. Next, the patch-size dependence of the order is studied under moderate inter-patch attraction, where the attractive bonding is thermally activated frequently. To systematically study the effect of the thermal activation and patch size, we also calculate the equilibrium orientational order against the attraction and patch size in a Monte Carlo simulation, because such thermally activated

† Electronic Supplementary Information (ESI) available: Simulation methods. Analysis procedures. Additional results. Movies of microscopy observation. See DOI: 10.1039/b000000x/

[a] *Department of Physics, Kyushu University, 812-8581 Fukuoka, Japan. Fax: 092 642 4177; Tel: 092 642 4177; E-mail: iwashita@phys.kyushu-u.ac.jp*

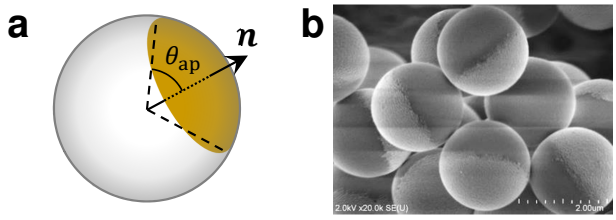

Fig. 1 One-patch particles. (a): A schematic drawing of a particle with a circular patch. $\boldsymbol{n}$ is the unit vector directed from the center of the particle to the center of the patch. (b): An SEM image of particles with a hemispherical patch. A bright region is a gold patch. Particle diameter $d = 2.0$ μm, and patch thickness h_0 = 50 nm.

states have not been considered in the theoretical work.[14] The patch-size dependence of the order in both simulation and experiment reveals the common ordering mechanism in them, and also suggest the selective fomation of a particular cluster by nonuniform inter-patch attraction. The commonalities and differences of the order with similar systems, and the effect of patch–substrate attraction are also studied.

2 Methods

2.1 Experiment

The method of preparing particles and solvent is the same as that in our previous work[8] except for patch-size control.

2.1.1 Particle preparation. A layer of gold with thickness h_d = 30–60 nm was deposited on a hemisphere of monodisperse silica particles (Hyprecica, UEXC), having diameter $d = 0.99$ or 2.04 μm and dispersion $\simeq \pm 3\%$ (see Fig. 1 (b)). Hereafter d is mainly written as 1.0 and 2.0 μm for simplicity. A circular patch smaller than the hemisphere was produced by chemical etching.[25] A patch is thickest at the center and becomes thinner toward its edge. In the following, the "thickness" of a patch, h_0, is that at the center of the patch, and the patch size is defined by θ_{ap}. θ_{ap} is measured by scanning electron microscopy (SEM) (e.g., Fig. 1 (b)), and patch thickness is estimated as $h_0 = h_d(1-\cos\theta_{ap})$.[25] The gold surface was modified with sodium-3-mercapto-propanesulfonate (97%, Wako) to prevent irreversible aggregation between gold patches.

2.1.2 Sample preparation and interaction control. The particles were dispersed in a binary mixture of 2,6-lutidine (99%, Sigma-Aldrich) and pure water (18.2 M Ω) at their critical composition, 28.6 wt% lutidine/water. This solvent shows a "lower critical solution temperature"-type phase separation and the critical temperature $T_c \simeq 34^\circ$C.[26] In the single-phase region near T_c, inter-particle interaction due to solvent criticality depends on the surface chemistry of particles and increases monotonically with approaching T_c.[27–30] This attraction can be used to control the inter-patch attraction of patchy particles.[8,24] In our system, the attraction between the hemispherical gold patches is stronger than that between bare surfaces and can be continuously tuned via temperature, allowing reversible control of aggregation via the sticky patches.

The particle dispersion was confined in a wedge-shaped cell composed of two cover glasses. The particles accumulated at the tip under acceleration provided by a centrifuge, and formed a densely packed monolayer. The lattice constant of the triangular lattice was 1.07 and 2.08 μm for $d = 0.99$ and 2.04 μm, respectively (cf. Fig. 3 (a)).

The top and bottom confinement surfaces of the cell were both hydrophobic for spontaneous ordering in Sections 3.1.1 and 3.2 or hydrophobic and hydrophilic respectively for induced ordering in Section 3.1.2. A hydrophilic cover glass was prepared by high-temperature treatment at 500°C for 3 hours, and a hydrophobic cover glass was prepared by modifying the surface with perfluorodecyltriethoxysilane (97%, Sigma-Aldrich).[31] No attraction was observed between a patch and a hydrophobic surface in our experiment. For a hydrophilic surface, patch–substrate attraction was observed at lower temperatures than T_c within ~ 0.2 K of T_c. A sample was observed with an optical microscope having a 40× objective lens while controlling the sample temperature with a stage (10021, Linkam Scientific Instruments).

2.2 Simulation

A standard Monte Carlo simulation was carried out to calculate the equilibrium orientational order of one-patch particles for inter-patch attraction e_b and patch size θ_{ap} (see ESI for details †). Spherical particles with a circular patch are arranged on a two-dimensional triangular lattice and can rotate three dimensionally. There are 1840 particles in the rectangular simulation box and they are subject to periodic boundary conditions.

We adopted a simple interaction composed of the orientation-dependent part of the Kern and Frenkel model.[32] In this interaction, there is a pairwise attractive potential (depth $e_b > 0$) only when the contact point between two neighboring particles is included in their patches. Other combinations of patch and non-patch surfaces do not give rise to an interaction.

The total number of simulation steps for each e_b and θ_{ap} is more than 10 times the number of steps at which the average cluster size N_{avg} reaches a steady value. Particles interacting with each other via patches are regarded as bonded, and the size of a cluster, N, is defined as the number of particles in the cluster. Four independent simulation runs were carried out for

each condition, and the results were averaged in analysis.

3 Results and discussions

3.1 Experiment: orientational order in hemispherically patched particles

3.1.1 Spontaneous ordering. After the preparation of a sample, hemispherical patches of particles aggregated in a close-packed monolayer, and the particles formed short linear clusters even around room temperature as shown in Fig. 2 (a) and (b). The aggregating patches exhibited rotational fluctuation; i.e. they slipped across each other's surfaces. The patches were sometimes thermally activated and aggregated with a different patch/patches (cf. the movie corresponding to Fig. 2 (b) in ESI†). These behaviors of aggregation suggest that the aggregating patches were at the secondary minimum of the Derjaguin–Landau–Verwey–Overbeek (DLVO) potential, and the potential depth was a few k_BTs; solvent criticality would induce negligible interaction around room temperature, $\Delta T \sim -8.0$ K.[27] The interaction is discussed later together with the results of simulations.

Self-assembly into such linear clusters via the attraction of hemispherical patches has been reported for particle dispersion.[8] A hemispherical patch can establish three attractive bonds with neighboring patches (cf. Section 1), and all the patches establish three bonds in a fully bonded double-strand linear cluster (cf. Fig. 2 (d)). Thus, the linear cluster is favored in terms of internal energy. In the following, we mainly consider the results with $d = 1.0$ μm particles, because structural relaxation in $d = 2.0$ μm particles is relatively slow even at room temperature; rotation is slower and inter-patch attraction is stronger for larger particles.[33]

Next we increased the temperature of the sample in Fig. 2 (b) to increase inter-patch attraction. From $\Delta T = -0.8$ K, at which the behavior of particles is little changed from that at room temperature, the temperature increased slowly at a rate of $<$0.01K/min on average; heating at 0.01 K/min was suspended for 5–10 min several times to make observations at constant temperature. Approaching T_c, the structural relaxation slowed, and at $\Delta T = -0.3$ K, the recombination of patches became fairly scarce, indicating inter-patch attraction was sufficiently stronger than k_BT (Fig. 2 (c)).

In Fig. 2 (c), the development of a zigzag stripe pattern from Fig. 2 (b) is observed. The zigzag stripe pattern is a parallel packing of fully bonded double-strand linear clusters as shown in Fig. 2 (d), where the maximum number of inter-patch bonds is attained as described above. This pattern is expected as the equilibrium orientational order for a large patch and strong attraction.[14] As shown in the inset of (c), there is periodic zigzag undulation in a linear cluster. Linear clusters are longer and their parallel alignment is more obvious in (c) than in (b).

In Fig. 2 (c), however, the zigzag stripe order is fairly short ranged even for such a slow approach to T_c. Figure 2 (e) and (f) represents the direction of linear clusters in Fig. 2 (b) and (c) respectively by color, and thus, a similarly colored domain corresponds to a monodomain of stripe order (see ESI for image processing†). Monodomains grow only slightly from Fig. 2 (e) to (f). We consider that the pattern in (c) is trapped in a metastable state upon relaxing into a better-ordered zigzag stripe pattern. Several theoretical and numerical works have reported that patchy particles are easily trapped in metastable states upon self-assembly.[7,22,23]

3.1.2 Induced ordering via solvent phase separation. When the critical solvent is heated above T_c, it phase-separates into water-rich and lutidine-rich phases. In this section a hybrid cell composed of a hydrophilic bottom surface and hydrophobic top surface was used, and the water-rich phase thus favors the bottom and the lutidine-rich phase the top. Therefore, the interface between the two phases would be parallel to the cell surfaces.

When a sample was heated above T_c, the pattern with a short-range zigzag stripe order described in the previous section transformed into a homogeneous hexagonal array (Fig. 3 (a)). Next, when a sample was cooled back into the one-phase state of the solvent, $T < T_c$, monodomains with a zigzag stripe pattern appeared via a nucleation-and-growth-like process (Fig. 3 (b) to (c)), predominantly from defects or grain boundaries of the hexagonal array (see arrowed domains in Fig. 3 (b)). Finally, a highly ordered zigzag stripe pattern formed as shown in Fig. 3 (d) and Fig. 4 (a), where spontaneous recombination of patches was rarely observed owing to the large attraction near T_c. There is an obvious difference in the monodomain size of the zigzag pattern between Fig. 2 (f) and Fig. 4 (b).

The mechanisms of the pattern transformation are considered as follows. At a vertical interface between phase-separated liquid phases in a hydrophobic cell, it was observed that a gold patch was in a water-rich phase and the bare surface was in a lutidine-rich phase (cf. supplementary Fig. C †), indicating surface activity of the particles. The energy of adhesion of a colloidal surfactant to a liquid interface is usually much higher than k_BT,[34,35] and the pattern transformation to Fig. 3 (a) indicates that the adhesion overwhelms the inter-patch attractive interaction.[24] Thus, homeotropic alignment of the particle, in which a gold patch faces the bottom, is realized by the preference of the patch for the water-rich phase (see the first drawing in Fig. 3 (e)).

Next, when the two phases consolute, patches begin attracting each other via the strong interaction close to T_c. Additionally, consolution kinetics might be coupled with patch–patch aggregation. When a stripe pattern appeared, aggregat-

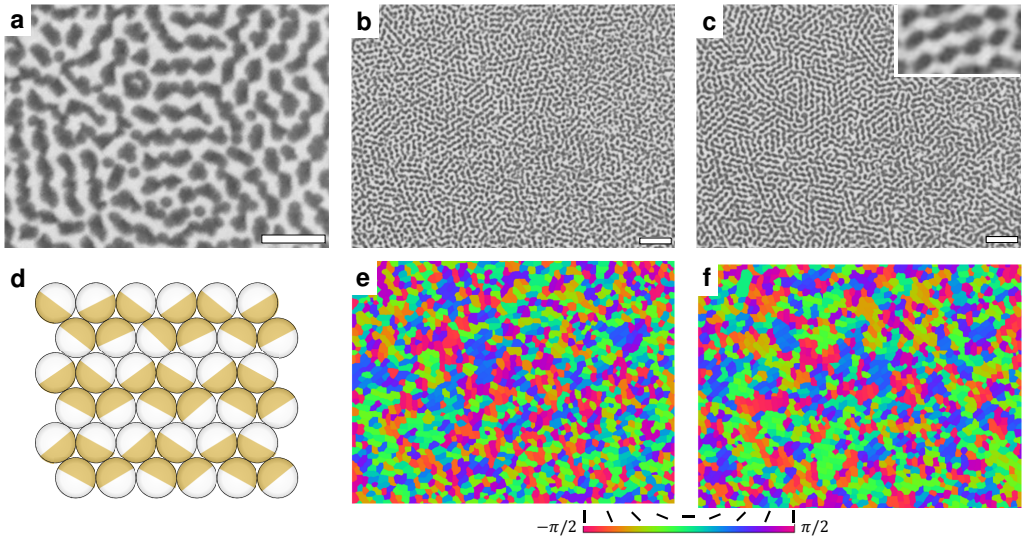

Fig. 2 Patterns of two-dimensionally close-packed particles with a hemispherical patch. (a) to (c) are microscopy images, in which a patch appears dark and the bare surface is not resolved. (a): Short linear clusters at $\Delta T = -8.0$ K. $d = 2.0$ μm and $h_0 = 50$ nm. (b): Short linear clusters at $\Delta T = -8.9$ K for $d = 1.0$ μm and $h_0 = 30$ nm. (c): Linear clusters at $\Delta T = -0.3$ K. The inset is a magnified image. (d): A schematic drawing of the zigzag stripe pattern. Patches, here brown hemispheres, are directed horizontally for simplicity; actual directions are three dimensional. The zigzag undulation in aggregating patches is considered to be independent between neighboring linear clusters. Between the second and third clusters from the top, the undulations are in phase but can be shifted by one particle. The direction of undulation patterns can be the opposite as shown by the first and second clusters. (e): Color plot of the direction of linear clusters in (b). (f): Color plot of the direction of linear clusters in (c). A common color bar for (e) and (f) is shown below the subfigures. Scale bars: 10.0 μm. Movies corresponding to (b) and (c) are available in ESI†.

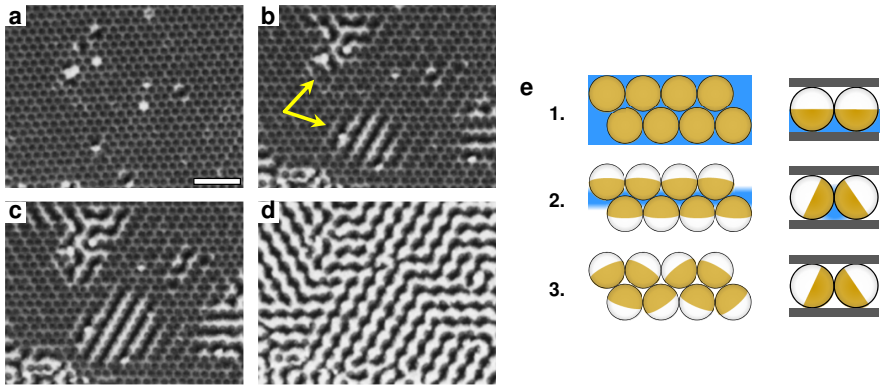

Fig. 3 Zigzag stripe pattern formation upon consolution of phase-separated solvent. (a) to (d): Sequential microscopy images upon cooling at -0.1 K/min. $\Delta T = 0.1$ K in (a), -0.1 K in (b) and (c), and -0.3 K in (d). $d = 2.0$ μm and $h_0 = 50$ nm. Scale bar: 10.0 μm. (e): Schematic drawings of the pattern formation process. Drawing 1 corresponds to (a), drawing 2 to (b) and (c), and drawing 3 to (d). The left drawings are the bottom view and the right drawings are the side view. An inverted microscope was used for observation. The water-rich phase is depicted in blue. A movie of the process from (a) to (d) is available in ESI.†

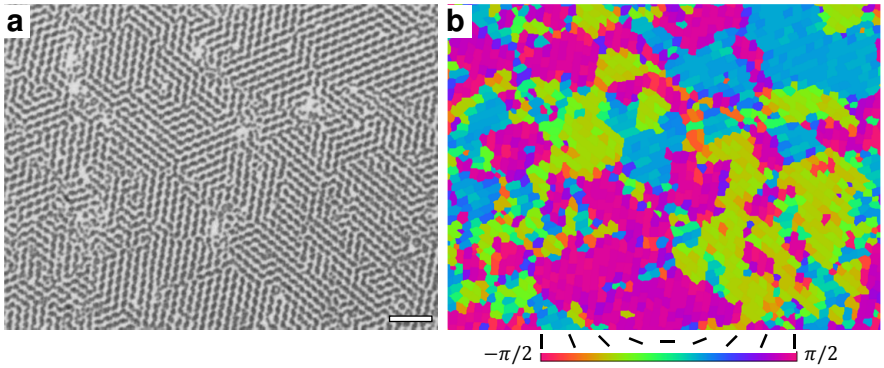

Fig. 4 Highly ordered zigzag stripe pattern at $\Delta T = -0.2$ K for $d = 1.0$ μm and $h_0 = 30$ nm. (a): Microscopy image. Scale bar: 10.0 μm. (b): Color plot of the direction of linear clusters in (a). A movie of the formation process of (a) is available in ESI.†

ing patches in a linear cluster showed no undulation at first as shown in Fig. 3 (c), and shortly later, a zigzag undulation formed. We suppose a dewetting-like process as in the second drawing in Fig. 3 (e), although the actual consolution dynamics are beyond the scope of this contribution. Additionally, after the consolution, a patch tilted toward the bottom as in the third drawing in Fig. 3 (e), because of a criticality-induced attraction between hydrophilic surfaces.[36]

In the current work, the directional growth of the zigzag stripe domain plays a key role in realizing the highly ordered state. The ordering kinetics are possibly coupled with consolution kinetics of the phase-separated solvent. The inter-patch and patch–substrate interactions caused by phase-separating solvent have also been studied for a similar system in ref.[24], although there are some differences such as surface properties of the particle and solvent criticality. The assembly behavior of particles might be controlled more by modifying the interaction via those conditions.[37]

3.1.3 Analysis of stripe order. A zigzag stripe pattern has a stripe or two-dimensional lamellar order composed of double-strand linear clusters in which patchy and bare surfaces are segregated from each other (see Fig. 2 (d)). In this section, we mainly consider stripe (or lamellar) order, not zigzag undulation in a linear cluster.

We first describe the characteristic defects of the order. Figure 5 (a) and (b) shows elementary dislocations, a node and end (or edge) of linear clusters, corresponding to $-1/2$ and $1/2$ disclination in a lamellar phase, respectively.[38]

Figure 5 (c) to (f) shows four types of grain boundaries between two stripe domains. Figure 5 (c) shows the array of ends of aggregating patches. In (c), bright regions (i.e., bare surfaces) form nodes. The pattern in Fig. 5 (f) appears as the brightness-inversion of (c); i.e., aggregating patches form nodes in (f). In Fig. 5 (d), showing an array of ends of aggregating patches, the two domains are parallel but shifted hor-

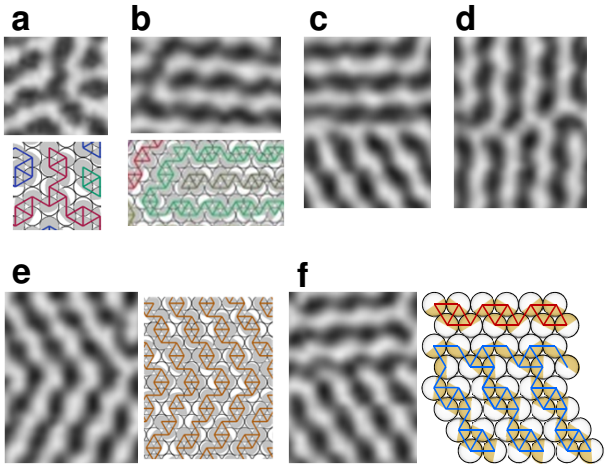

Fig. 5 Characteristic defect structures in a stripe pattern. (a) and (b): Elementary dislocations. (a) is a node and (b) is an end. (c) to (f): Grain boundaries between two stripe monodomains. Possible schematic structures are shown in (a), (b), (e) and (f), where patches are depicted in gray or brown, and bonds connecting centers of neighboring particles are drawn when the patches aggregate.

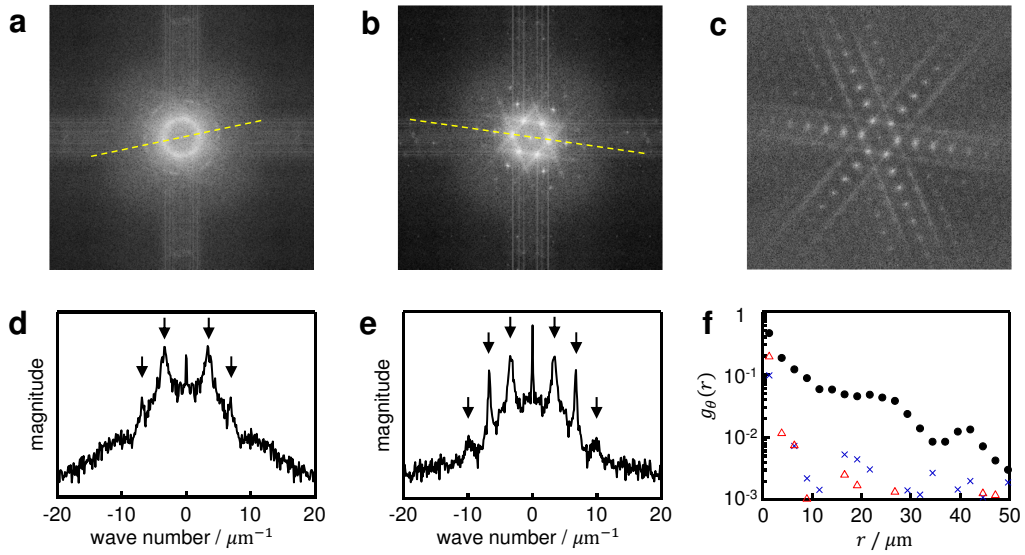

Fig. 6 Image analysis of patterns in hemispherically patched particles. (a) and (b): Power spectrum obtained by Fourier transformation of Fig. 2 (c) and Fig. 4 (a), respectively. (c): Power spectrum obtained after skeletonizing Fig. 4 (a). Six-fold symmetry of the periodic linear array of spots is more evident than that in (b). (d) and (e): Intensity profile along the dashed line in (a) and (b), respectively. Each line crosses spots of the power spectra, although the spots in (a) are obscure. (f): Radial directional correlation of linear clusters. Symbols correspond to the images as follows: (×, Fig. 2 (b)), (△, Fig. 2 (c)) and (•, Fig. 4 (a)).

izontally by one particle. In Fig. 5 (e), there is no defect between the two angled domains; such structure is known as a curvature wall in a lamellar phase.

Next, to quantify the order of the patterns obtained by spontaneous and induced ordering, we analyzed the patterns as follows (see ESI for details of the procedure†). The Fourier transformation of a pattern was calculated to show the symmetry and characteristic length scale of a pattern (Fig. 6 (a), (b) and (c)). We also calculated the radial directional correlation of linear clusters to quantify the spatial expansion of a stripe monodomain (Fig. 6 (f)). A topological quantity, the number of ends of linear domains, gives a measure of the connectivity of linear clusters.

In the Fourier transformation, a region with dimensions of 65.2 μm × 65.2 μm was analyzed to investigate the order in a monodomain of hexagonal packing. Figure 6 (b) is the power spectrum of the pattern obtained by induced ordering in Fig. 4 (a), and Fig. 6 (e) is a line profile of the intensity along the peaks in Fig. 6 (b). The six-fold pattern composed of a linear array of periodic peaks in Fig. 6 (b) reflects stripe patterns in three directions in the triangular lattice. The symmetry of the six-fold mosaic pattern of stripe domains is emphasized more in Fig. 6 (c), obtained from the skeletonized pattern of Fig. 4 (a) (see ESI for the image†).

From the peak positions, we obtain the stripe period $\lambda = 1.87$ μm, which is slightly greater than the calculated period for close-packed particles $\lambda \simeq 1.8$ μm; in a zigzag stripe pattern, λ is the distance between the centers of neighboring linear clusters. Thus, $\lambda = \sqrt{3}d = 1.71$ μm for spherical particles, and the thickness of two patches, $\sim 0.1\mu$m, should be added (cf. Fig. 2 (d)). For $d = 2.0$ μm in Fig. 3 (d), $\lambda = 3.68$ μm in the experiment and $\lambda \simeq 3.6$ μm is calculated for close-packed particles. Additionally, the secondary minimum of the DLVO potential is typically within tens of nanometers from a surface and the thermal vibration of a particle gives rise to additional repulsion. Thus, the slightly larger λ in the experiment is quite reasonable for the close-packed particles.

The six-fold peaks are blurred for spontaneous ordering in Fig. 2 (c), and the pattern appears almost isotropic in Fig. 6 (a). The peak positions indicated by arrows in Fig. 6 (d) are the same as those in Fig. 6 (e); however, the third cannot be identified clearly in (d). These features indicate very local, short-range stripe order in Fig. 2 (c). The power spectrum of a pattern at low temperature (e.g., Fig. 2 (b)) is almost the same as that of Fig. 2 (c).

Next we calculated the radial directional correlation of linear clusters, g_θ, using the nematic order parameter. Directional correlation between two segmented parts of linear clusters is measured as $2\cos^2\Delta\theta - 1$, where $\Delta\theta$ is the angular difference. $g_\theta(r)$ is the average of the correlation for all pairs of two segments at a distance $r \le r_{ij} < r + \Delta r$, where r_{ij} is the distance between segment i and j and $\Delta r = 2.5$ μm. When all segments in the r-range are parallel, $g_\theta(r) = 1$, whereas the value is zero when the segments are directed randomly.

In Fig. 6 (f), directional correlation is observed only at short range, $\sim 2\ \mu$m, for spontaneous ordering at $\Delta T = -8.9$ K (Fig. 2 (b)). Here $g_\theta(r)$ below $\sim 10^{-2}$ is within statistical error, and negative $g_\theta(r)$ does not appear in the plot. For $\Delta T = -0.3$ K (Fig. 2 (c)), the correlation at short range increases, whereas the spatial range remains short. For induced ordering in Fig. 4 (a), the directional correlation at short range is strongest in the three plots, and the spatial range is fairly large: $g_\theta(r)$ maintains significant correlation until about 30 μm. This length coincides with the size of monodomains in Fig. 4 (a).

In the analyses above, the development of a pattern in spontaneous ordering is not identified clearly. The development was observed in the connectivity of linear clusters or aggregating patches; i.e., the number of ends, $n_{\rm end}$. At $\Delta T = -8.9$ K in spontaneous ordering in Fig. 2 (b), $n_{\rm end}$ = 0.24 μm^{-2}, whereas the value decreases to 0.16 μm^{-2} at $\Delta T = -0.3$ K in Fig. 2 (c). For the highly ordered pattern in Fig. 4 (a), $n_{\rm end}$ = 0.14 μm^{-2}. The connectivity of clusters (i.e., aggregation of patches) greatly improved with approaching $T_{\rm c}$ in spontaneous ordering, indicating that aggregation, or attractive bonding, between patches was promoted by the increase in attraction. Additionally, relatively minor improvement of connectivity from a short-range ordered pattern to a highly ordered pattern suggests that bonding had fairly well developed already in the spontaneous ordering near $T_{\rm c}$, although the pattern was trapped in a metastable state.

As described above, the stripe pattern and its formation mechanism have significant similarities to a general stripe or two-dimensional lamellar phase;[38,39] e.g., a block in a polymer is segregated in block copolymer systems, and in surfactant systems, the hydrophobic or hydrophilic part of a molecule is segregated together with water and/or oil, resulting in a lamellar phase under proper conditions. However, there is a fundamental difference. Patchy particles are so close-packed that rearrangement of their relative positions is completely prohibited (cf. hexagonal close-packing in Fig. 3 (a)); thus, the order is almost purely orientational. In a general stripe or lamellar phase, however, molecules possess both translational and orientational order, or at least translational order. A curvature wall is an interesting example of a possible difference; the condition of each patchy particle at the curve is identical to that at the straight part (see the schematic drawing in Fig. 5 (e)). In a general stripe/lamellar phase, curvature alters the local spatial symmetry around a molecule and gives rise to bending energy.

3.2 Experiment: patch-size dependence

In this section, we describe patch-size dependence of orientationally ordered patterns in a hydrophobic cell. Figure 7 (a) is an example of a pattern formed when $d = 2.0\ \mu$m, patch size $\theta_{\rm ap} = 59^\circ$ with $\pm 6\%$ dispersion and $\Delta T = -14$ K. The major-

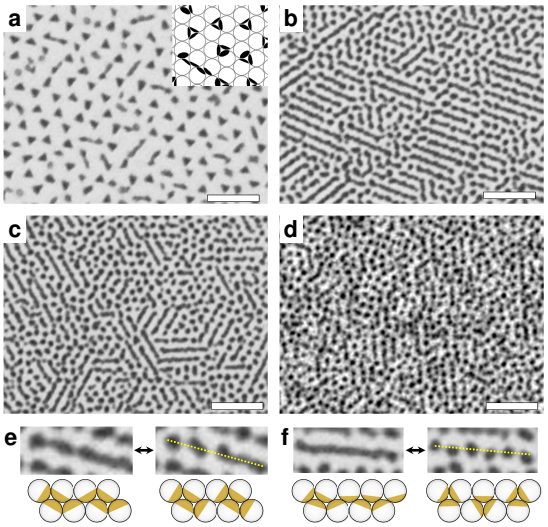

Fig. 7 Patch-size dependence of orientational order observed with an optical microscope. $d = 2.0\ \mu$m in (a) and 1.0 μm in (b) to (d). (a): $\theta_{\rm ap} = 59^\circ$, $\Delta T = -14$ K and $h_0 = 29$ nm. The inset is a schematic drawing of triangular trimers and a linear cluster. (b): $\theta_{\rm ap} = 77^\circ$, $\Delta T = -14$ K and h_0 = 47 nm. (c): $\theta_{\rm ap} = 70^\circ$, $\Delta T = -14$ K and h_0 = 40 nm. (d): $\theta_{\rm ap} = 52^\circ$, $\Delta T = -0.2$ K and h_0 = 23 nm. In this sample, most particles did not cluster around room temperature. Contrast in the image is largely enhanced because the patch was small and thin. (e): Recombination of particles between a linear cluster and rhombic tetramers observed in (b). (f): Recombination of particles between a linear cluster and triangular trimers observed in (c). Note that we could not specify inter-patch bonding in a linear cluster in this sample; the schematic linear cluster is a possible example. Scale bars: 10 μm. Movies corresponding to (b) and (c) are available in ESI.†

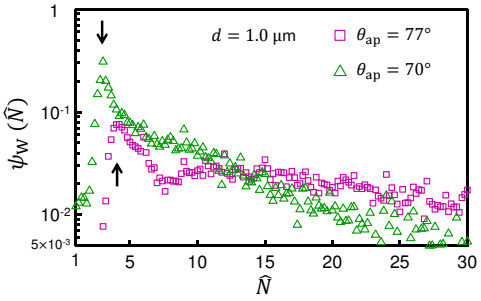

Fig. 8 Cluster-size distribution estimated from microscopy observation for Fig. 7 (b) ($\theta_{\rm ap} = 77^\circ$) and (c) ($\theta_{\rm ap} = 70^\circ$). $\psi_{\rm w}(\hat{N})$ is the probability that a particle belongs to the cluster of size $\hat{N}$. The peaks of a trimer for $\theta_{\rm ap} = 70^\circ$ and tetramer for $\theta_{\rm ap} = 77^\circ$ are indicated by arrows.

ity of clusters were a triangular trimer as shown in the inset,[40] and some other clusters, such as linear clusters and monomers, were also observed. The tiling of triangular trimers is the theoretically predicted equilibrium order for θ_{ap} of $\sim 30^\circ$–60°.[14] The relaxation of clustering was, however, fairly slow for this size of particle as described earlier. Thus, the clusters would reflect the kinetic process of packing by centrifuge.

To investigate equilibrium patterns with small patches, we used particles for which $d = 1.0\ \mu$m. The patch size $\theta_{ap} = 77^\circ \pm 3\%$, $70^\circ \pm 3\%$ and $52^\circ \pm 10\%$, and the thickness $h_0 = 47$, 40 and 23 nm respectively, from Fig. 7 (b) to (d). The interaction energy of a particle with its nearest neighbors depends on the patch size and thickness, because the former determines the possible bond number and the latter determines the van der Waals attraction between patches. Under the conditions in Fig. 7 (b) to (d), particles were clustered but thermally activated rather frequently (cf. corresponding movies in ESI†), and we thus presume the cluster state to be in equilibrium.

For $\theta_{ap} = 77^\circ$ in Fig. 7 (b), small clusters and relatively long clusters coexisted, and the ratio of small clusters increased with a decrease in θ_{ap} as shown in Fig. 7 (c) and (d). For $\theta_{ap} = 52^\circ$ in (d), most clusters were in fact small. For the sample in Fig. 7 (b) and (c), two characteristic recombination processes between small clusters and a linear cluster were observed. In Fig. 7 (e), a linear cluster with zigzag undulation decomposed into linearly aligned tilted small clusters, and *vice versa*. In Fig. 7 (f), small clusters are shifted from the center of a linear cluster in alternative directions when a linear cluster decomposes. The former recombination suggests that, as schematically drawn in Fig. 7 (e), a zigzag cluster is thermally activated predominantly into rhombic tetramers. Such a decomposition of a zigzag cluster has been reported for a more dilute system;[8] in a zigzag cluster, the tetramers are connected to each other only by a single bond. The latter recombination seen in Fig. 7 (f) suggests that a linear cluster decomposes into triangular trimers directed "upward" and "downward" alternatively.

By carefully observing the recombination, the process in Fig. 7 (e) was found more for $\theta_{ap} = 77^\circ$ than for $\theta_{ap} = 70^\circ$, and the process in Fig. 7 (f) was found more for $\theta_{ap} = 70^\circ$. These observations are supported by the cluster size distributions in Fig. 8. A cluster size (i.e., the number of aggregating patches), $\hat{N}$, is roughly estimated from the area of a dark region (see ESI for details†). The area depends not only on the number of patches but also on the vertical directions of patches, and the distribution of area, or $\hat{N}$, is thus not discrete. The estimated sizes in the plots of Fig. 8 are obtained from more than 10 images. In the plots, tetramers and trimers are clearly abundant for $\theta_{ap} = 77^\circ$ and 70° respectively, and they coexist with large clusters indicated by the exponential-like long tail. Such a tail is observed in step growth polymerization or for living polymers as a result of probabilistic linear aggregation of unit structures,[39] which is consistent with the active thermal recombination of bonding in the experiments here.

The results in this section are discussed again together with the results of simulation.

3.3 Simulation

In the experiments under moderate inter-patch attraction (e.g., Fig. 2 (b) and Fig. 7 (b) to (d)), clusters were fairly polydisperse. Such thermally activated cluster states were not studied in previous theoretical work.[14] To compare directly with our experiments and study the patch-size and inter-patch-attraction dependence systematically, we calculate the steady states of the orientational order in a Monte Carlo simulation. The steady states are presumably in equilibrium; however, the possibility of the existence of more stable states cannot be excluded.

3.3.1 Without patch–substrate interaction. The patch size and the energy of inter-patch attractive bonding are θ_{ap} ranging from 6.0° to 90.0° in intervals of 6.0°, and e_b ranging from 0.0 to 10.0 k_BT in intervals of 1.0 k_BT, and $e_b = 1000 k_BT$. In this section, patch–substrate interaction is not considered; i.e., the order is purely determined by inter-patch attraction.

Figure 9 (a) to (c) shows snapshots of typical patterns under high inter-patch bonding energy, $e_b = 10.0 k_BT$. A zigzag stripe pattern, tiling of triangular trimers, and tiling of dimers appear, as in ref.[14]. Depending on the parameters, however, a disordered pattern composed of polydisperse clusters form. A stripe order of shorter range than that in Fig. 9 (a) appears in Fig. 9 (d) and (e), where segregation of patches in a double-strand linear cluster is still observed but zigzag undulation of patches is rather disturbed. Figure 9 (f) is a mixture of dimers, triangular and non-triangular trimers, linear clusters and even monomers.

By considering the ground states (see, e.g., Fig. 9 (a) to (c)) and calculated equilibrium states, we classify each cluster as a monomer, dimer, triangular trimer, large cluster ($N \geq 8$), or other cluster. The size criterion for the large cluster is related to the stripe order, because most clusters of $N \geq 8$ are linear and an increase in the number of such linear clusters generates stripe order. Other cluster includes tetramers to heptamers and non-triangular trimers.

The formation of the five cluster states against patch size and bond energy is summarized in the diagram presented in Fig. 10 (a). Each symbol in Fig. 10 (a) corresponds to the cluster occupying maximum ψ_w for each set of θ_{ap} and e_b as explained in the legend. Here ψ_w is calculated as the ratio of the number of particles belonging to each cluster state to the total number of particles in the system, 1840. The stripe order of linear clusters is judged by eye. In Fig. 10 (c) to (e), ψ_w

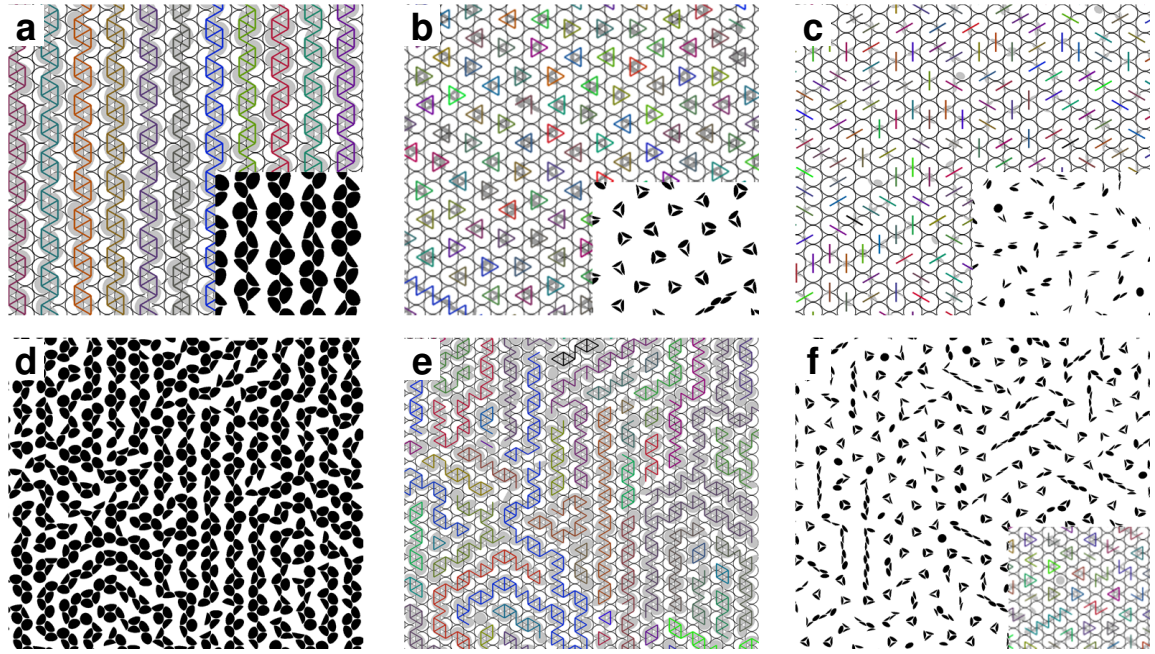

Fig. 9 Typical patterns obtained by Monte Carlo simulation. (a): Almost perfectly ordered monodomain of a zigzag pattern. $\theta_{ap} = 78°$. (b): Random tiling of triangular trimers. $\theta_{ap} = 42°$. (c): Random tiling of dimers. $\theta_{ap} = 30°$. $e_b = 10.0 k_B T$ from (a) to (c). (d) and (e): A less-ordered stripe pattern. $e_b = 4.0 k_B T$ and $\theta_{ap} = 78°$. (f): A polydispersed cluster state, mainly composed of triangular trimers and linear clusters. $e_b = 6.0 k_B T$ and $\theta_{ap} = 42°$. In (a), (b), (c), (e) and the inset of (f), the bond connecting the centers of two neighboring particles is depicted when the particles interact with their patches, and a different color is given to each cluster. In (d), (f) and the insets of (a), (b) and (c), patches are depicted in black to compare them with microscopy images. The images are cropped and magnified from the original images of 1840 particles, and the scales are the same for (a) to (c) or (d) to (f). Other patterns are shown in ESI.†

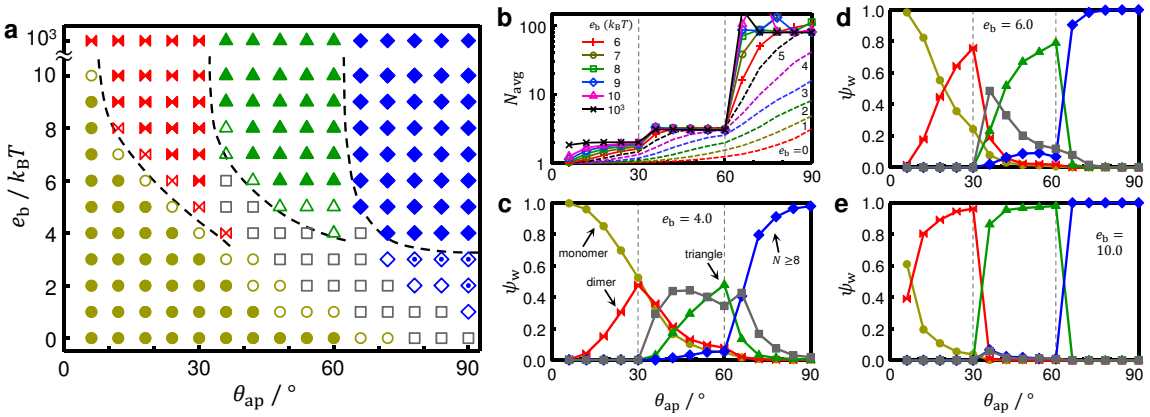

Fig. 10 Patch size and attraction dependence of the cluster state in simulation. (a): Diagram of the cluster states: (monomer, ○), (dimer, ⋈), (triangular trimer, △), (large clusters of $N \geq 8$, ◇) and (other clusters, □). Filled symbols and a diamond with a dot represent that $\psi_w > 2/3$, and a filled diamond indicates stripe order. Dashed curves are guides for the eye to emphasize the boundaries between the cluster states. (b): Dependence of the average cluster size, N_{avg}, on θ_{ap} and e_b. Dashed lines correspond to $e_b = 0.0$ to $5.0 k_B T$ from the bottom to top. e_b values of marked lines are given in the figure. The large fluctuation around $N_{avg} \sim 100$ is due to the periodic boundary conditions: the lattice axis is parallel to the y-axis and maximum N is 80 in that direction, whereas in directions of the other lattice axes, all particles can belong to a linear cluster; i.e., maximum $N = 1840$. (c) to (e): ψ_w of the cluster states in (a) is plotted against θ_{ap}. $e_b = 4.0$, 6.0 and $10.0 k_B T$ from (c) to (e), respectively.

of each of the five cluster states is plotted against θ_{ap} for some e_b.

For high bond energy (i.e., when internal energy is dominant to free energy), the ground states are realized (cf. Fig. 9 (a) to (c)), as determined by the maximum number of possible bonds per patch as described in Section 1. ψ_w of each ground state is almost unity for $e_b = 10^3 k_B T$.

With a decrease in bond energy, clusters become polydisperse from the lower θ_{ap} boundary of each ground state as shown in Fig. 10 (c) to (e), where the boundaries are indicated by dashed lines. The boundaries of the regions in which the three cluster states occupy the largest fraction shift to larger θ_{ap} for smaller e_b in Fig. 10 (a), and finally the three regions disappear. Figure 10 (a) is similar to the phase diagram in ref.[14]; however, there are qualitative differences in the theoretical framework. Specifically, in our system, cluster states, or orientational orders, are not assumed in advance and translational entropy is not included at all.

Our results show that the transition of a cluster state becomes continuous with decreasing e_b, as suggested by the smoothed profile of the average cluster size for small e_b in Fig. 10 (b). For each cluster state, however, a discontinuity in the fraction still remains under small e_b. ψ_w of triangular trimers in Fig. 10 (c), for example, gradually increases with increasing θ_{ap} from the lower boundary of the ground states and suddenly decreases from the upper boundary.

The patch size dependence of the transitions is qualitatively explained by the effect of rotational entropy.[13] When θ_{ap} of a patch approaches the lower limit of each possible bond number, 60° for three bonds and 30° for two bonds as described above, the range of possible rotational fluctuation of a patch approaches zero; i.e., the entropic cost for establishing the maximum number of bond increases, which makes the full bonding of a patch unstable. Thus, with an increase in the relative contribution of the entropy to free energy due to a decrease in e_b, the transition of cluster states becomes continuous and the boundaries shift.

3.3.2 With large patch-substrate attraction. In addition to the simulation above, we also calculated steady states of one-patch particles under strong patch–substrate attraction, because a patch is strongly bound to the hydrophilic substrate in the formation of a zigzag pattern as described in Section 3.1.2. Thus, an infinitely strong patch–substrate attraction is added to the simulation method; i.e., a patch–substrate bond does not rupture once established. θ_{ap} ranges from 45° to 90.0° in intervals of 3.0°, and e_b ranges from 0.0 to 10.0 $k_B T$ in intervals of 1.0 $k_B T$.

Results of analyses and typical patterns are shown in Fig. 11 and Fig. 12, respectively. Apparently, the zigzag stripe pattern is the equilibrium orientationally ordered state even with strong patch–substrate attraction.

The general trends of orientational orders against the inter-patch attraction and patch size are similar to those without patch–substrate attraction, except for the position of the boundaries between the cluster states. For large e_b, rather discrete sequential transition of a pattern from the zigzag stripe to triangular trimers to dimers is observed with a decrease in θ_{ap}. However, the relative θ_{ap} ranges of the three states are significantly different from those in Fig. 10 (a). The dimer region fairly narrows, whereas the stripe region narrows only slightly. The θ_{ap} range, again, corresponds to the ground state determined by the maximum number of bonds per patch. The effective patch size (i.e., the length of the arc on the horizontal plane where particles interact) is smaller than the actual size of a patch because of the tilt induced by patch–substrate bonding. Therefore, by considering the geometry, the boundaries between three and two, two and one, and one and zero bonds per patch are calculated as $\theta_{ap} = 63.4°$, 49.1° and 45.0°, respectively, consistent with the boundaries in Fig. 11 (a).

Near the boundary of θ_{ap}, as actually shown in Fig. 12 (a) and (c), the vertical orientation of a patch is almost constant because the inter-patch bonds are established near the edge of a patch and the orientation can thus fluctuate only slightly. With a decrease in θ_{ap} toward the lower boundary of each ground state, a cluster state becomes polydisperse as described in the previous section because of the rotational entropy.

These results suggest that a strong patch–substrate attraction simply tilts a patch toward the substrate and reduces the effective patch size, which affects the ground states non-monotonically. However, only the two extreme conditions of a substrate are compared; orientational order with a moderate patch–substrate interaction remains to be studied.

3.4 Comparison between experiment and simulation

Our simulations show that the zigzag stripe pattern is the equilibrium ordered state for large θ_{ap} and e_b, with either no or strong patch–substrate attraction. For the hemispherically patched particles in our experiment, the decrease in the number of ends of linear clusters indicates the development of linear clusters when inter-patch attraction increased, whereas a zigzag stripe pattern developed only slightly as suggested by the small increase in orientational order (see Section 3.1.1). The highly ordered zigzag pattern was realized only by induced ordering via solvent phase separation (see Section 3.1.2). These results illustrate that, for patchy particles, controlling ordering kinetics is important to avoid particles being trapped in metastable states during self-assembly.[7,22,23]

Inter-patch attraction can be roughly estimated by comparing the results of experiment and simulation. In the simulation, the stripe order disappears below $\sim 4 k_B T$. Thus, in the pattern with short-range stripe order in Fig. 2 (b) (i.e., for 1 μm particles with a $\sim$ 30 nm-thick hemispherical patch

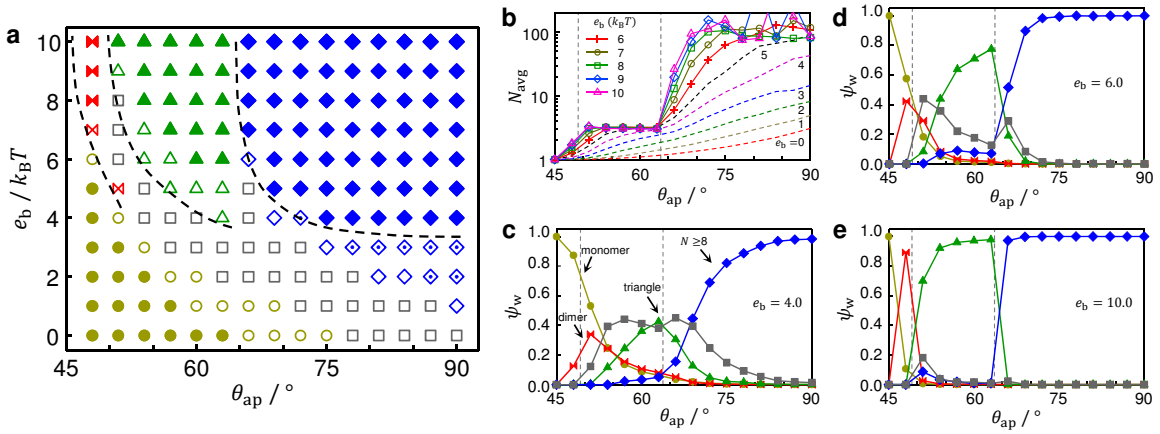

Fig. 11 Patch size and attraction dependence of the cluster state in simulation with a strong patch–substrate attraction. Notations in the graphs are the same as those in Fig. 10. (a): Diagram of the cluster states. (b): Dependence of the average cluster size on θ_{ap} and e_b. The large fluctuation around $N_{avg} \sim 100$ is due to the periodic boundary conditions. (c) to (e): ψ_w of each cluster state in (a) is plotted against θ_{ap}. $e_b = 4.0$, 6.0 and $10.0 k_B T$ from (c) to (e), respectively. Dashed lines are the θ_{ap} boundaries between the ground states.

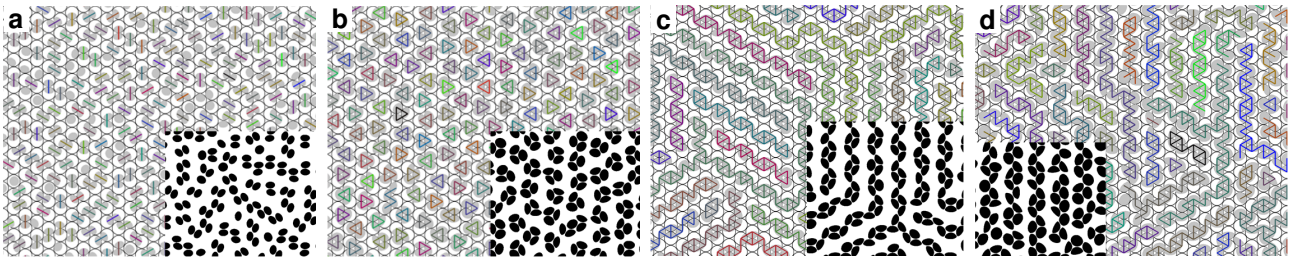

Fig. 12 Typical equilibrium patterns obtained by simulation with a strong patch–substrate attraction. (a) to (c): $e_b = 10.0 k_B T$, and $\theta_{ap} = 48°$, 63° and 66° respectively from (a) to (c). (d): $e_b = 4.0 k_B T$ and $\theta_{ap} = 75°$.

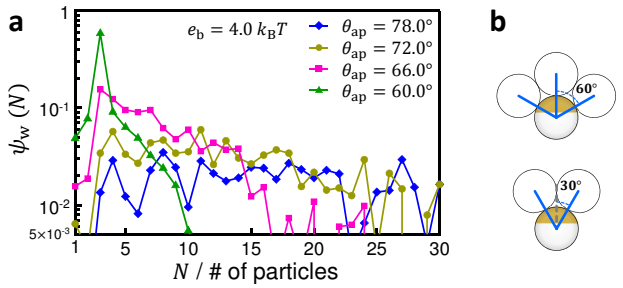

Fig. 13 Cluster size distribution in simulation with moderate inter-patch attraction in (a) and schematic drawing of bond angles in (b). (a): $e_b = 4.0 k_B T$ without patch–substrate attraction. θ_{ap} of each plot is shown in the picture. (b): Bond angles on a patch. top: three bonds, bottom: two neighboring bonds.

without criticality-induced interaction), which was presumably in equilibrium under thermal activation, the depth of the inter-patch attractive potential would be a few $k_B T$.

To consider patch-size dependence, the experimentally observed patterns in Fig. 7 (b) to (d) are compared with the equilibrium patterns calculated under moderate inter-patch attraction, because the patterns were presumably in equilibrium in these experiments as described earlier.

Both in the experiment (see Fig. 7 (b) to (d)) and simulation (see Fig. 9 and 10), the abundance of small clusters, typically $N \leq 4$, increased with decreasing θ_{ap}. The distribution of the cluster size, however, has a different feature. In the experiment, a prominent peak of trimers or tetramers is observed over the exponential-like decay following the peak (see Fig. 8). In simulation, such a prominent peak over a long-tail decay is not observed as shown in Fig. 13 (a); the plots of $\theta_{ap} = 60.0°, 66.0°$ and $72.0°$ show exponential-like monotonic decay after the peak at $N = 3$ or 4, although the plots are scattered because of statistics and the internal structure of a zigzag cluster.[41]

A possible origin of the difference is direction-dependent inter-patch attraction caused by nonuniform thickness of a patch. With the angle measured from the center of a patch, θ, the thickness $h(\theta) \simeq h_0(\cos\theta - \cos\theta_{ap})$ for $\theta \leq \theta_{ap}$.[25] Because of the thickness dependence of van der Waals attraction, the attractive potential of a patch decreases toward the edge. On the other hand, the average bond angle is 60° for the outer two bonds among three bonds, and it is 30° for the two neighboring bonds on a patch (Fig. 13 (b)), and the former bonds should thus be weaker than the latter ones. When a linear cluster decomposes into triangular trimers or rhombic tetramers, this difference in bond energy would compensate the loss of internal energy to some extent, because a linear cluster requires more three-bond patches than the small clusters (cf. Fig. 7 (e)). Therefore, compared with clustering under uniform inter-patch attraction in Fig. 13 (a), the population of the small clusters is enhanced in the experiment, Fig. 8.

In addition to the above, there are other factors possibly associated with the orientational order in the experiment. The thermal vibration of a cluster would be smaller and more anisotropic for linear clusters than for the coexisting small clusters. This difference might affect the spatial distribution of the clusters, or even cause phase separation between linear and small clusters; Figure 7 (b) and (c) might suggest the directional order of linear clusters and the nonuniform distribution of linear and small clusters. Dynamic effects such as anisotropic phonon transfer dependent on orientational order would also be interesting. The small shape anisotropy of a particle due to the gold cap could also participate in inter-particle interaction in such a dense system. These aspects are to be considered in future work.

4 Conclusions

Our study experimentally shows the importance of ordering kinetics in attaining a highly ordered state of patchy particles even for orientational order.[7,22,23] The directional growth of a zigzag pattern plays a key role in the ordering, as known for the crystallization of isotropic colloids or even molecules and atoms.[42] By directly comparing the steady states, presumably equilibrium states, of orientational order between experiment and simulation, common ordering mechanisms are clarified: the ground states are determined by the number of possible bonds per patch via the patch size,[14] and a transition between the states becomes continuous with decreasing inter-patch attraction because of the effect of rotational entropy on bonding.[13] On the other hand, a larger population of a particular cluster in the experiment would be an example that a cluster state can be selectively formed by nonuniform inter-patch attraction.

These orientational orders induced by patchy particles have various commonalities with similar orders in liquid crystals and ferrofluid,[38,39] whereas the orders are purely orientational in close-packed patchy particles. The orientational order of dipoles or spins in condensed matter is also well known, although their orientational order is usually inseparable from positional order. Additionally, dipolar interaction favors head-to-tail arrangement, as opposed to head-to-head or tail-to-tail arrangement of patchy particles. Thus, there is the great possibility that condensed patchy particles will become a novel mesostructured material having unique functionalities derived from the purely orientational order and its response to the external conditions including applied field.

Acknowledgement

We thank Prof. Hirotsugu Kikuchi, Prof. Yasushi Okumura and the Center of Advanced Instrumental Analysis, Kyushu University for SEM observations, and Dr. Kyohei Takae for relevant discussions. We gratefully acknowledge support from JSPS KAKENHI under grant no. 23740319 and Kurata Grants.

Notes and references

1 S. C. Glotzer and M. J. Solomon, *Nat. Mater.*, 2007, **6**, 557.
2 K. J. Lee, J. Yoon and J. Lahann, *Curr. Opin. Colloid In.*, 2011, **16**, 195.
3 A. Walther and A. H. E. Mueller, *Chem. Rev.*, 2013, **113**, 5194–5261.
4 C. Kaewsaneha, P. Tangboriboonrat, D. Polpanich, M. Eissa and A. Elaissari, *Colloids Surf., A*, 2013, **439**, 35–42.
5 Q. Chen, J. K. Whitmer, S. Jiang, S. C. Bae, E. Luijten and S. Granick, *Science*, 2011, **331**, 199.
6 G. Munao, Z. Preisler, T. Vissers, F. Smallenburg and F. Sciortino, *Soft Matter*, 2013, **9**, 2652–2661.
7 Z. Preisler, T. Vissers, F. Smallenburg, G. Munao and F. Sciortino, *J. Phys. Chem. B*, 2013, **117**, 9540–9547.
8 Y. Iwashita and Y. Kimura, *Soft Matter*, 2013, **9**, 10694–10698.
9 Q. Chen, S. C. Bae and S. Granick, *Nature*, 2011, **469**, 381.
10 Z. Zhang and S. Glotzer, *Nano Lett.*, 2004, **4**, 1407.
11 F. Romano, E. Sanz, P. Tartaglia and F. Sciortino, *J. Phys.: Condens. Matter*, 2012, **24**, 064113.
12 T. Vissers, Z. Preisler, F. Smallenburg, M. Dijkstra and F. Sciortino, *J. Chem. Phys.*, 2013, **138**, 164505.
13 X. Mao, Q. Chen and S. Granick, *Nat. Mater.*, 2013, **12**, 217–222.
14 H. Shin and K. S. Schweizer, *Soft Matter*, 2014, **10**, 262–274.
15 F. Sciortino and E. Zaccarelli, *Curr. Opin. Solid State Mater. Sci.*, 2011, **15**, 246–253.
16 B. Ruzicka, E. Zaccarelli, L. Zulian, R. Angelini, M. Sztucki, A. Moussaid, T. Narayanan and F. Sciortino, *Nat. Mater.*, 2011, **10**, 56–60.
17 E. Bianchi, R. Blaak and C. N. Likos, *PCCP*, 2011, **13**, 6397–6410.
18 N. Dorsaz, L. Filion, F. Smallenburg and D. Frenkel, *Faraday Discuss.*, 2012, **159**, 9.
19 S. C. Weber and C. P. Brangwynne, *Cell*, 2012, **149**, 1188–1191.
20 P. Li, S. Banjade, H.-C. Cheng, S. Kim, B. Chen, L. Guo, M. Llaguno, J. V. Hollingsworth, D. S. King, S. F. Banani, P. S. Russo, Q.-X. Jiang, B. T. Nixon and M. K. Rosen, *Nature*, 2012, **483**, 336–U129.
21 D. J. Beltran-Villegas, B. a. Schultz, N. H. P. Nguyen, S. C. Glotzer and R. G. Larson, *Soft Matter*, 2014, doi:10.1039/c3sm53136h.
22 O. A. Vasilyev, B. A. Klumov and A. V. Tkachenko, *Phys. Rev. E*, 2013, **88**, 012302.
23 C. S. Dias, N. A. M. Araujo and M. M. Telo da Gama, *Soft Matter*, 2013, **9**, 5616–5623.
24 C. Yu, J. Zhang and S. Granick, *Angew. Chem. Int. Ed*, 2014, **53**, 1.
25 Q. Chen, E. Diesel, J. K. Whitmer, S. C. Bae, E. Luijten and S. Granick, *J. Am. Chem. Soc.* , 2011, **133**, 7725.
26 C. A. Grattoni, R. A. Dawe, C. Yen Seah and J. D. Gray, *J. Chem. Eng. Data*, 1993, **38**, 516.
27 C. Hertlein, L. Helden, A. Gambassi, S. Dietrich and C. Bechinger, *Nature*, 2008, **451**, 172.
28 R. Okamoto and A. Onuki, *Phys. Rev. E*, 2011, **84**, 051401.
29 R. Okamoto and A. Onuki, *J. Chem. Phys.*, 2012, **136**, 114704.
30 T. F. Mohry, A. Maciolek and S. Dietrich, *J. Chem. Phys.*, 2012, **136**, 224902.
31 H. Sugimura, A. Hozumi, T. Kameyama and O. Takai, *Surf. Interface Anal.*, 2002, **34**, 550–554.
32 N. Kern and D. Frenkel, *J. Chem. Phys.*, 2003, **118**, 9882–9889.
33 In general, the secondary minimum of the DLVO potential is within tens of nanometers from a surface,[?] which is much shorter than the particle radius. Thus, the interaction is almost proportional to the radius following the Derjaguin approximation.
34 B. P. Binks and P. D. I. Fletcher, *Langmuir*, 2001, **17**, 4708–4710.
35 Y. Hirose, S. Komura and Y. Nonomura, *J. Chem. Phys.*, 2007, **127**, 054707.
36 The attraction to the bottom due to hydrophilicity should be stronger for a patch than a bare surface, because the preference to water is larger for a patch as described above, although a bare surface is also hydrophilic.
37 R. Okamoto and A. Onuki, *Phys. Rev. E*, 2013, **88**, 022309.
38 P.-G. de Gennes and J. Prost, *The Physics of Liquid Crystals*, Clarendon Press, Oxford, 1993.
39 T. A. Witten and P. A. Pincus, *Structured Fluids: Polymers, Colloids, Surfactants*, Oxford University Press, New York, 2004.
40 Q. Chen, J. Yan, J. Zhang, S. C. Bae and S. Granick, *Langmuir*, 2012, **28**, 13555.
41 A zigzag linear cluster is an array of rhombic tetramers connected with a single bond as described earlier. Thus, the internal energy of a zigzag cluster has local minima at $N = 4n$, where n is natural number, resulting in peaks of ψ_w at the N.[8] The peaks are actually observed in this work at $N = 4$ and 8 for $\theta_{ap} = 78.0°$, and possibly for 72.0°, in Fig. 13 (a).
42 U. Gasser, *J. Phys.: Condens. Matter*, 2009, **21**, 203101.

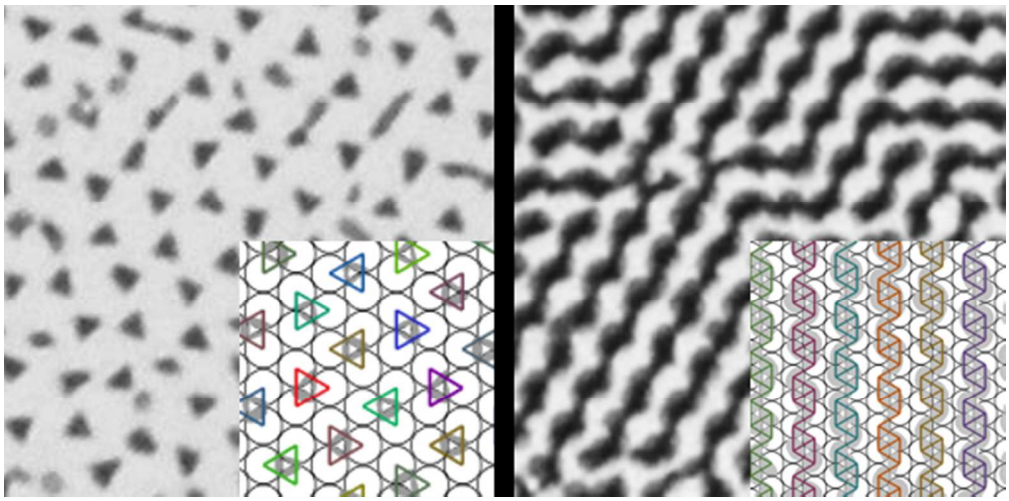

Various orientational orders of one-patch colloidal particles were realized experimentally by controlling ordering kinetics. Comparison of them with the equilibrium orders calculated by simulation reveals the ordering mechanism.